DOI: 10.1002/anie.201206948

Stereodynamics

Orientation Effect in the Low-Energy Electron Attachment to the Apolar Carbon Tetrafluoride Molecule**

*Lei Xia, Xian-Jin Zeng, Hong-Kai Li, Bin Wu, and Shan Xi Tian**

Stereodynamics of the molecular fragmentation by energetic particle impact provides essential information about the interaction between the projectile and target, which has been the central topic of chemical reactions.[1] Versatile information on the collision stereodynamics may degrade seriously by measuring the spherically averaged cross-sections because of the randomly oriented target molecules, but can benefit from the oriented target molecules that are prepared prior to the collision. Up to date, the polar molecules in gas phase can be oriented or aligned by an electrostatic field[2] or in a linear-polarized laser field.[3] Except for some sophisticated methods (e.g., the stimulated Raman pumping[4]), the alignment or orientation of apolar molecules (without permanent dipole moment) is still a challenge in experiments. For the randomly oriented molecules in some cases, a similar effect of alignment or orientation could be derived from the significant anisotropy of the polar-angle-resolved differential cross-sections (DCS).[5–7] However, the orientation effect is scarcely observed in slow collision reactions. During the slow approaching of the projectile, the spatial anisotropy of the projectile–target interaction potential is usually believed to be averaged out because of the molecular rotations of the target.

In contrast to the above-mentioned conventional wisdom, the orientation effect in the low-energy electron attachment to the apolar molecule CF_4 is observed in our anion velocity image mapping experiments. The CF_4 molecule is randomly oriented in a field-free environment during attachment. Up to now, only some simple linear apolar molecules (H_2, D_2, N_2, and CO_2) were investigated for the orientation effect in medium- (dozens of electronvolts) or high-energy (several hundreds to more one thousand electronvolts) electron collisions.[5–7] In this work, the low-energy (no more than 6 eV) electron attachment to CF_4 shows that electron capture can be strongly influenced by the target molecular orientation, leading to specific distributions of the fragment momenta. In the impulsive dissociation, the axial-recoil approximation[8] has been well validated. The intermediate state of the dissociative precursor usually follows the fragment trajectories parallel or perpendicular to the initial molecular axis.

A temporary negative ion CF_4^- formed by electron attachment is just this type of dissociative precursor and may decay through two complementary dissociation pathways, $CF_4^- \rightarrow F^- + CF_3$ (channel a) and $F + CF_3^-$ (channel b)[9,10] with appearance energies of 3.7 and 4.4 eV,[11] respectively. The yield efficiency curves of the F^- and CF_3^- fragments produced in these two dissociative electron attachment (DEA) processes were recorded and a broad band in each curve was found.[9–11] At the lower energies of about 6 eV, channels a and b were suspected to experience the common resonance state $^2T_2$ of CF_4^-,[10,11] while the lower resonance state $^2A_1$ was mainly responsible for the autodetachment $CF_4^- \rightarrow e^- + CF_4$.[10] Although the DEA dynamics has been partly revealed by angular distributions (at 6.7 eV for F^- and 6.1 eV for CF_3^-) of the anionic fragments, there are a lot of uncertainties because those measurements were performed in the small angular θ range of 15 to 110°.[10] Such limitation is due to the spatial restriction of the rotating ion detector used in their turn-table arrangement.[10] The full picture of DEA dynamics should be promising by using more advanced experimental techniques. The state-of-the-art anion velocity image mapping method recently developed in our group[12] and by others[13] can realize measurements of both the DCS of the anionic fragment in a full angular range (θ = 0–360°) and the kinetic energy distributions simultaneously.

The time-sliced images (azimuth angle ϕ of about 0°) of the F^- velocity were recorded at electron energies of 5.3, 5.5, 6.0, and 7.0 eV (Figure 1); while the images of CF_3^- were recorded at 5.5, 6.0, 6.5, and 7.0 eV (Figure 2). Because of the different kinetic energies of the anionic fragments and the small size of the detector (its effective diameter is 40 mm), the images were contracted or enlarged by biasing the electrode voltages for the faster F^- and the slower CF_3^- anions. The kinetic energies or velocities obtained from the images were calibrated with values available in the literature.[12–14]

As shown in Figure 1, the central higher intensity of F^- indicates that most anions have low kinetic energies (0–0.5 eV, increasing slightly at higher attachment energies) and the larger image size implies a higher kinetic energy or a larger velocity of the F^- ion. At the outer ring, which corresponds to kinetic energies higher than 0.8 eV, a remarkable anisotropy of the F^- distribution is observed although the ion intensities are much weaker (less than 10% of the central intensity). The high-momentum distribution appears partially on the image recorded at 6.0 eV but completely disappears at 7.0 eV. The distribution is suspected to be located outside the detector, which is due to its large momentum value or another dissociation channel. The images of the CF_3^- momentum are distinctly different from those of F^-. As shown in Figure 2, the low kinetic-energy components are not observed for the CF_3^-

[*] L. Xia, X.-J. Zeng, H.-K. Li, B. Wu, Prof. Dr. S. X. Tian
Hefei National Laboratory for Physical Sciences at the Microscale and Department of Chemical Physics
University of Science and Technology of China
Hefei, Anhui 230026 (China)
E-mail: sxtian@ustc.edu.cn

[**] This work is financially supported by the NSFC (grant number 21273213), MOST (grant number 2011CB921401), and FRFCU.

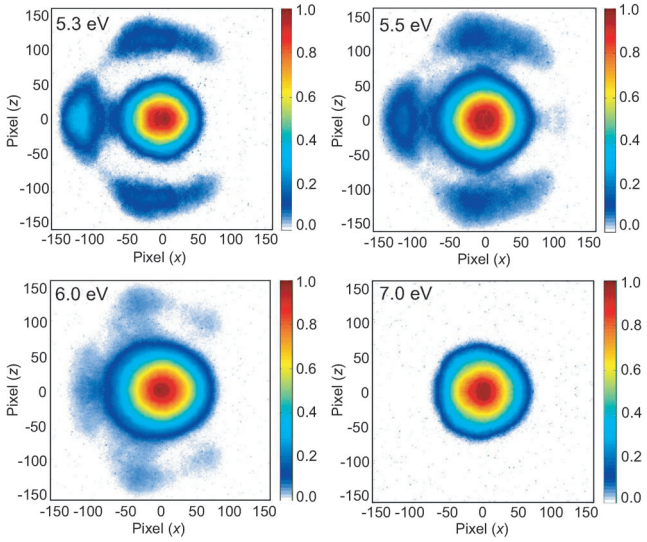

Figure 1. Slice images of F^- recorded at 5.3, 5.5, 6.0, and 7.0 eV. The intensities are normalized and the electron incident direction is from left to right.

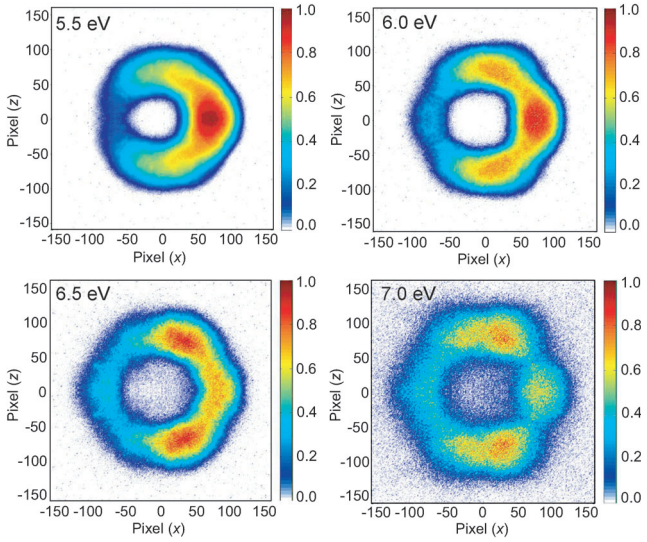

Figure 2. Slice images of CF_3^- recorded at 5.5, 6.0, 6.5, and 7.0 eV. The intensities are normalized and the electron incident direction is from left to right.

momentum distributions; while the high-momentum (corresponding to a kinetic energy higher than 0.3 eV) distributions show significant forward-scattering characteristics (except for that at the attachment energy of 7.0 eV). With increase in the electron energy, the images are also enlarged, indicating higher kinetic energies of the CF_3^- fragment. In previous studies,[9,10] the authors conjectured that CF_4^- formed by electron attachment on the repulsive potential-energy curve of the resonance state $^2T_2$. Then impulsive dissociations led to the ground-state products, $F^-(^1S_0) + CF_3(^2A_1)$ and $F(^2P) + CF_3^-(^1A_1)$. If the excess electron statistically follows the fluorine atom or carbon trifluoride in the complementary dissociations, the velocities of the fragments should be satisfied with $\vec{v}(CF_3^-) = \vec{v}(CF_3)$ and $\vec{v}(F^-) = \vec{v}(F)$; furthermore, the kinetic correlation between F^- and CF_3^- fragments measured in the experiments should obey the momentum conservation, $v(F^-) = [m(CF_3^-)/m(F^-)]v(CF_3^-) \approx 3.63\ v(CF_3^-)$. Such dissociation mechanism is potentially supported by the forward-scattering pattern of the F^- image together with the backward-scattering pattern of the CF_3^- image.

The kinetic correlation between the two fragments at an attachment energy of 5.5 eV will be discussed in detail. As shown in Figure 3a, the outer annular ring covers the

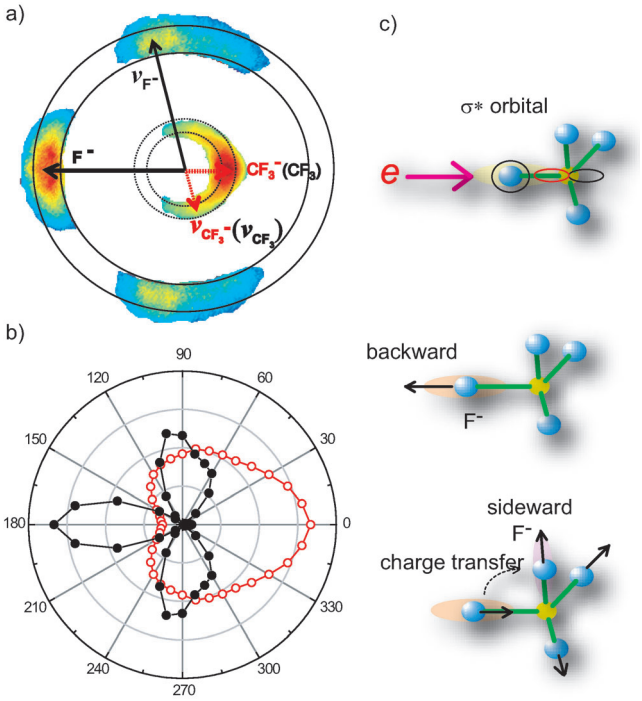

Figure 3. a) The kinetic correlation between the faster F^- and CF_3^- fragments: here $v(CF_3) = v(CF_3^-)$ in which CF_3 is the product of $CF_4^- \rightarrow F^- + CF_3$; two annular areas (recorded at the electron energy of 5.5 eV and with intensity renormalizations) correspond to the kinetic energies of 0.90–1.60 eV (F^-) and 0.25–0.45 eV (CF_3^-). b) The angular distributions of F^- (solid circles), CF_3^- (empty circles), and the ion intensities are obtained with integrations of the ion signals in the above-mentioned two annular areas and normalized. c) The orientation effect on the F^- momentum distributions.

intensities of the F^- ions with kinetic energies of 0.90 to 1.60 eV, which corresponds to the main distributions of the CF_3^- kinetic energies from 0.25 to 0.45 eV (the inner annular ring). Therefore, their velocity (also kinetic energy) values are in a proportion of $v(F^-)/v(CF_3^-) \approx 3.63$; moreover, the angular distributions observed in Figure 3a indicate that these two fragments are departing within the momentum conservation rule. The DCSs in terms of the angle θ of F^- and CF_3^- are plotted by integration of the ion signals in the respective annular areas and plotted in Figure 3b. Besides the strongest intensities at the backward (F^-) and forward (CF_3^-) directions, there are also two lobes in the angle ranges at 60–120° and 240–300° (sideward distributions). We will give more explanations to the above-mentioned anisotropies.

The resonance state $^2T_2$ of CF_4^- has been identified as the excess electron occupation at the virtual molecular orbital $5t_2$ (consisting of the empty $3s_F$ and $2p_C$ atomic orbitals, see Figure 3c).[9–11] This orbital has C–F σ* antibonding character. The beginning of the present DEA process should prefer the electron-attacking trajectories along one local C–F bond (depicted as the upper panel in Figure 3c), and the dissociative precursor CF_4^- ($^2T_2$) is formatted. This CF_4^- precursor subsequently dissociates, leading to a remarkable backward-scattering image pattern of the F^- distributions (alternatively, the forward-scattering of CF_3^-) by stretching this C–F bond (see the middle panel in Figure 3c). In other words, the specific molecular orientation in which one C–F bond faces the incoming electron is significantly favored in the attachment, although the target molecule is randomly oriented. On the other hand, the previous studies indicated that the molecular vibrations of four modes (ν_1, C–F symmetric stretching; ν_2 and ν_4, degenerate deformations; ν_3, C–F asymmetric stretching) could be activated at the $^2T_2$ resonance state; in particular, the excitation of the C–F asymmetric stretching (ν_3) was predominated in the electron collision with CF_4.[15] The two broad lobes in the angle ranges of 60–120° and 240–300° observed in Figure 3b could be interpreted as: when the excess electron is captured and occupies one local σ* C–F antibonding orbital, the electron–nuclei motion coupling leads to the excitation of the C–F asymmetric stretching (ν_3); thereafter, the negative charge may partially transfer to the other σ* C–F antibonding orbitals with assistance of the asymmetric stretching vibrations. Therefore, the sideward distributions of the F^- fragment should be attributed to the cleavage of those weakened C–F bonds (see the lowest panel of Figure 3c). Accordingly, some CF_3^- fragments can also be produced in the complementary dissociation process. The orientation effect on the electron attachment to CF_4 was proposed but is ambiguous because of its measurements in a limited angle range.[10] Herein, a complete and much clearer picture about this orientation effect is given, owing to the merits of the present experimental technique.[12]

The low-energy F^- fragments depicted in the center of the images in Figure 1 show the isotropic distributions for different electron energies, implying that the related dissociations should occur around their threshold energies. The appearance energy of 3.7 eV of F^- should be attributed to fast fragmentation CF_4^-–$F^- + CF_3$ (channel a).[11] Although the thermodynamic threshold of this channel is about 1.18 eV (estimated by the electron affinity of the fluorine atom of 3.40 eV[16] and the dissociation energy $D(F–CF_3)$ of 5.58 eV[17]), the dissociations to the electronic excited-state CF_3 ($^2A_2''$) or the higher states should be inaccessible.[10] The residual energies subtracting the translational parts (0–0.5 eV) of the slow F^- fragments should be in the range of 3.6–5.8 eV for attachment energies from 5.3 to 7.0 eV. The residual energies can be possibly found: to produce the high rovibrational states of CF_3 ($^2A_1$) or in the three-body dissociation $CF_4^- \rightarrow F^- + CF_2 +$ F with a threshold of 5.97 eV.[10]

As shown in Figure 2, the momentum distribution of CF_3^- at an attachment energy of 7.0 eV is distinctly different from the distribution recorded at lower energies, namely, the orientation effect declines dramatically. With the increase in the electron-incident energy, the vibrational-excitation fraction of the total electron attachment cross-section decreases.[18] Therefore, only the electronic wavefunctions of the initial ($^1A_1$ of CF_4) and intermediate ($^2T_2$ of CF_4^-) states are considered in the following analysis. Azria et al.[19] extended the theory about the fragment angular distribution[8] for polyatomic molecules on the basis of the work by O'Malley and Taylor,[20] who originally developed their theory for diatomic molecules under the axial-recoil approximation. Here we follow this description for randomly oriented molecules. The angular distribution is basically determined by pure electronic coupling with the continuum. The angular distribution of CF_3^- with kinetic energies of 0.25–0.65 eV recorded at 7.0 eV is plotted in Figure 4, and the

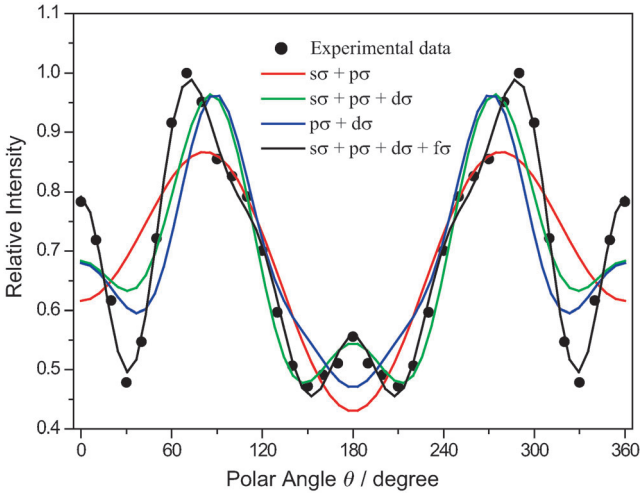

Figure 4. Curves fitted to the experimental data for the angular distribution of CF_3^- with kinetic energies of 0.25–0.65 eV recorded at an electron energy of 7.0 eV.

experimental data are fitted using various linear combinations for the electron partial waves (up to an angular moment $l = 3$, that is, s, p, d, f partial waves). The combination set of sσ + pσ scattering amplitudes can reproduce two strong peaks around 90 and 270°, but fails for the forward- (0°) and backward-scattering (180°) peaks. The forward-scattering distribution is improved by using the pσ + dσ scattering amplitudes. The sσ + pσ + dσ scattering amplitudes can give a much better description, but they are still insufficient for the fine structures of the angular distribution, for example, the minima around 30 and 330°, and the peak positions around 70 and 290°. The best one is the combination of sσ + pσ + dσ + fσ scattering amplitudes, in which the component ratio of each partial-wave scattering amplitude is sσ:pσ:dσ:fσ = 1:0.53:0.78:0.66. By comparing these fitting results, one can find that the dσ and fσ amplitudes are responsible for the forward-scattering while the backward-scattering is mostly determined by the sσ amplitude.

In summary, we observed the fragment orientation in the low-energy electron dissociative attachments to the apolar molecule CF_4. With increase in the electron incident energy,

this orientation effect distinctly declines and the anisotropic distribution of CF_3^- is interpreted as the result of the interference among the sσ, pσ, dσ, and fσ asymptotic amplitudes. The electron attachment or trapping as the beginning of the DEA process can be remarkably influenced by the spatial orientation of the target molecule. The present findings recall the more rigorous treatment of the projectile–target interaction in the low-energy collision reactions. Moreover, this stereospecificity should be universal in electron capture and intermolecular charge transfer.

Experimental Section

The experimental details can be found in Ref. [12]. Briefly, an effusive molecular beam was emitted perpendicular to the pulsed low-energy electron beam from a homemade electron gun; the low-energy electrons (along the *x* axis) were collimated with a homogenous magnetic field produced by a pair of Helmholtz coils. The anionic fragment yields were periodically pushed out from the reaction area and then flew through the time-of-flight tube installed along the molecular beam (the *y* axis). Ten electrodes of the time-of-flight mass spectrometer were in charge of the spatial and velocity focusing of the anions. The volume of the anion fragments produced during one electron-beam pulse expanded in the three-dimensional space and formed a Newton sphere. Finally the anions were detected with three microchannel plates and a phosphor screen mounted on a flange in the *x*–*z* plane. The sliced images of the anionic Newton sphere were directly recorded with a CCD camera by applying a detection time-gate pulse (width about 35 ns) on the rear microchannel plate. The commercial gas-phase sample CF_4 with a purity of 99.9% was used in the experiments.

Received: August 28, 2012
Revised: November 8, 2012
Published online: November 26, 2012

Keywords: charge transfer · dissociative electron attachment · ion imaging · stereodynamics · velocity mapping

[1] R. D. Levine, *Molecular Reaction Dynamics*, Cambridge University Press, Oxford, **2005**.
[2] D. H. Parker, *Annu. Rev. Phys. Chem.* **1989**, *40*, 561; P. R. Brooks, E. M. Jones, *J. Chem. Phys.* **1966**, *45*, 3449; P. R. Brooks, *Science* **1976**, *193*, 11.
[3] H. Stapelfeldt, T. Seideman, *Rev. Mod. Phys.* **2003**, *75*, 543.
[4] G. O. Sitz, R. L. Farrow, *J. Chem. Phys.* **1994**, *101*, 4682; A. D. Rudert, J. Martin, W.-B. Gao, J. B. Halpern, H. Zacharias, *J. Chem. Phys.* **1999**, *111*, 9549; S. Cureton-Chinn, P. B. Kelly, M. P. Augustine, *J. Chem. Phys.* **2002**, *116*, 4837; N. C. M. Bartlett, D. J. Miller, R. N. Zare, D. Sofikitis, T. P. Rakitzis, A. J. Alexander, *J. Chem. Phys.* **2008**, *129*, 084312.
[5] O. Al-Hagan, C. Kaiser, D. Madison, A. J. Murray, *Nat. Phys.* **2009**, *5*, 59.
[6] J. Colgan, M. S. Pindzola, F. Robicheaux, C. Kaiser, A. J. Murray, D. H. Madison, *Phys. Rev. Lett.* **2008**, *101*, 233201; U. Werner, N. M. Kabachnik, V. N. Kondratyev, H. O. Lutz, *Phys. Rev. Lett.* **1997**, *79*, 1662.
[7] T. Weber, A. Czasch, O. Jagutzki, A. Muller, V. Mergel, A. Kheifets, J. Feagin, E. Rotenberg, G. Meigs, M. H. Prior, S. Daveau, A. L. Landers, C. L. Cocke, T. Osipov, H. Schmidt-Bocking, R. Dorner, *Phys. Rev. Lett.* **2004**, *92*, 163001; T. Weber, A. Czasch, O. Jagutzki, A. Muller, V. Mergel, A. Kheifets, E. Rotenberg, G. Meigs, M. H. Prior, S. Daveau, A. L. Landers, C. L. Cocke, T. Osipov, R. D. Muino, H. Schmidt-Bocking, R. Dorner, *Nature* **2004**, *431*, 437; M. Takahashi, N. Watanabe, Y. Khajuria, Y. Udagawa, J. H. D. Eland, *Phys. Rev. Lett.* **2005**, *94*, 213202; S. Bellm, J. Lower, E. Weigold, D. W. Mueller, *Phys. Rev. Lett.* **2010**, *104*, 023202.
[8] G. H. Dunn, *Phys. Rev. Lett.* **1962**, *8*, 62; R. N. Zare, *Mol. Photochem.* **1972**, *4*, 1.
[9] K. A. G. MacNeil, J. C. J. Thynne, *Int. J. Mass Spectrom. Ion Phys.* **1970**, *3*, 455; P. W. Harland, J. L. Franklin, *J. Chem. Phys.* **1974**, *61*, 1621; E. Illenberger, *Chem. Phys. Lett.* **1981**, *80*, 153; S. M. Spyrou, I. Sauers, L. G. Christophorou, *J. Chem. Phys.* **1983**, *78*, 7200; I. Iga, M. V. V. S. Rao, S. K. Srivastava, J. C. Nogueira, *Z. Phys. D* **1992**, *24*, 111; F. Weik, E. Illenberger, *J. Chem. Phys.* **1995**, *103*, 1406.
[10] Y. Le Coat, J.-P. Ziesel, J.-P. Guillotin, *J. Phys. B* **1994**, *27*, 965.
[11] S. V. K. Kumar, M. A. Rahman, S. Roy, *Int. J. Mass Spectrom.* **2008**, *277*, 57.
[12] B. Wu, L. Xia, H.-K. Li, X.-J. Zeng, S. X. Tian, *Rev. Sci. Instrum.* **2012**, *83*, 013108.
[13] H. Adaniya, B. Rudek, T. Osipov, D. J. Haxton, T. Weber, T. N. Rescigno, C. W. McCurdy, A. Belkacem, *Phys. Rev. Lett.* **2009**, *103*, 233201; N. Bhargava Ram, E. Krishnakumar, *J. Chem. Phys.* **2012**, *136*, 164308.
[14] B. Wu, L. Xia, Y.-F. Wang, H.-K. Li, X.-J. Zeng, S. X. Tian, *Phys. Rev. A* **2012**, *85*, 052709.
[15] A. Mann, F. Linder, *J. Phys. B* **1992**, *25*, 545 L. Boesten, H. Tanaka, A. Kobayashi, M. D. Dillon, M. Kimura, *J. Phys. B* **1992**, *25*, 1607.
[16] C. Blondel, C. Delsart, F. Goldfarb, *J. Phys. B* **2001**, *34*, L281.
[17] M. W. Chase, Jr., *J. Phys. Chem. Ref. Data* **1985**, *14*, Suppl. 1.
[18] J. Troe, T. M. Miller, N. S. Shuman, A. A. Viggiano, *J. Chem. Phys.* **2012**, *137*, 024303.
[19] R. Azria, Y. Le Coat, G. Lefever, D. Simon, *J. Phys. B* **1979**, *12*, 679.
[20] T. F. O'Malley, H. S. Taylor, *Phys. Rev.* **1968**, *176*, 207.

